

MRI-Based Large Deformation High Dimensional Mapping of the Hippocampus in Rats: Development and Validation of the Technique

R. Edward Hogan, MD,^{1*} Viviane Bouilleret, MD, PhD,^{2,3} Ying Rui Liu,² Lei Wang, PhD,⁴ John P. Williams, PhD,⁵ Bianca Jupp, PhD,² Damian Myers, PhD,² and Terence J. O'Brien, MD^{2,6,7}

Purpose: To report the detection of structural and functional biological changes in living animals using small animal in vivo MRI that complements traditional ex vivo histological techniques. We report the development and validation of the application of large deformation high dimensional mapping (HDM-LD) segmentation for the hippocampus in the rat.

Materials and Methods: High resolution volumetric T2 weighted MRI images were acquired at 4.7 Tesla from six male in-breed nonpileptic Wistar rats. Two HDM-LD segmentations of the hippocampus (automated 1 and automated 2) were compared with the manual segmentations of two investigators who independently segmented the hippocampi (manual 1 and manual 2).

Results: The mean overlap for the hippocampi between automated 1 and automated 2 for the right hippocampi was 94.4% (SD 1.0) and for the left hippocampi was 94.3% (SD 2.5), while the mean overlap between automated 1 and manual 1 for the right hippocampi was 91.4% (SD 1.3) and for the left hippocampi was 91.9% (SD 1.4). Mean values for absolute differences for comparisons of all the segmentations were the following: automated 1 versus automated 2, 3.2% (SD 1.0); manual 1 versus manual 2 6.82% (SD 5.22); automated 1 versus manual 1 13.0% (SD 1.8).

Conclusion: HDM-LD can be applied to obtain accurate and reproducible three-dimensional segmentations of the hippocampus from rat MR images. HDM-LD will be a useful tool for investigations of hippocampal structural changes in vivo in rat models of human disease.

Key Words: MRI; hippocampus; rat
J. Magn. Reson. Imaging 2009;29:1027–1034.
 © 2009 Wiley-Liss, Inc.

THE HIPPOCAMPUS PLAYS a central role in many different neuropsychiatric diseases, including epilepsy (1), schizophrenia (2), and Alzheimer's disease (3). This has led to extensive study of the hippocampus in animal models of neuropsychiatric disease (4,5). The recent rapid advances in the technology and availability of dedicated small animal in vivo imaging systems, specifically MRI, allows the detection of structural and functional biological changes in living animals, and complements traditional ex vivo histological techniques. A particular advantage of this approach is the ability to perform serial imaging of animals, increasing the power to track the ontogeny of the changes, their relationship to behavioral aspects of the disease, and potentially, the effect of interventions. The findings on postmortem histological examination can be correlated with the imaging results, and thus the respective advantages of the temporal versus spatial resolution of the two methods can be harnessed.

In both humans and animals, past investigators have used manual segmentation of the hippocampus on MR

¹The Department of Neurology, Washington University, St. Louis, Missouri.

²Departments of Medicine, The Royal Melbourne Hospital, The University of Melbourne, Parkville, Victoria, Australia.

³Department of Neurophysiology and Epilepsy, ApHp, CHU Bicetre, Paris, France.

⁴Department of Psychiatry, Northwestern University, Chicago, Illinois.

⁵The Howard Florey Institute, Parkville, Victoria, Australia.

⁶Department of Surgery, The Royal Melbourne Hospital, The University of Melbourne, Parkville, Victoria, Australia.

⁷The Royal Melbourne Hospital, The University of Melbourne, Parkville, Victoria, Australia.

Contract grant sponsor: Victorian Government Transport Accident Commission (TAC); Contract grant number: DP0023.

*Address reprint requests to: R.E.H., Washington University in St. Louis, Department of Neurology, 660 S. Euclid Avenue, Campus Box 8111, St. Louis, MO 63110. E-mail: hogan@wustl.edu

Received September 29, 2008; Accepted February 9, 2009.

DOI 10.1002/jmri.21766

Published online in Wiley InterScience (www.interscience.wiley.com).

images to determine hippocampal volumes (4,6,7). While the sensitivity for detecting hippocampal asymmetry of manual segmentation as compared to visual inspection is greater in some investigatory settings (8), manual segmentation is time consuming and requires expertise in the details of hippocampal anatomy for accurate segmentations. The difficulty in manual segmentations lies in the subjective interpretations of anatomical variations. The emerging field of Computational Anatomy (9) founded on general pattern theory provides tools and a frame work for accommodating and studying this variability (10–12). Large deformation high dimensional mapping (HDM-LD) is based on principles of computational anatomy, and uses the power of computer assisted shape recognition to identify general patterns within image data. An electronic reference atlas, which can be deformed according to the properties of a viscous fluid, is used to study a hippocampus of interest according to several defined landmarks. Computational anatomic techniques produce three-dimensional (3D) surface representations of the hippocampus with resolution at a subvoxel level, enabling visualization of details of hippocampal surface anatomy (13). HDM-LD extends analysis of longitudinal MRI imaging beyond the volumetric to subregional and morphometric analyses (1).

Several past studies have demonstrated the precision of deformation-based hippocampal segmentation of the hippocampus in humans (14,15). Haller et al (16) described a deformation-based hippocampal segmentation technique and verified the precision of this technique in normal subjects and schizophrenic patients. Hogan et al showed reproducibility of 92% overlap of sequential deformation-based hippocampal segmentations in subjects with epilepsy and mesial temporal sclerosis (15). HDM-LD identifies subtle neuroanatomical and longitudinal changes in diseases such as epilepsy, Alzheimer's disease, depression, and schizophrenia, that are not detectable with standard volumetric methods (3,17–19).

Using a high resolution volumetric acquisition MRI protocol, we have developed a technique for applying HDM-LD to perform segmentations of the rat hippocampus. To verify the precision of HDM-LD segmentation in the rat hippocampus, we compared HDM-LD segmentations with the manual segmentations of two investigators who independently segmented the hippocampi. These studies for validation of the HDM-LD technique were performed in six in-bred nonepileptic Wistar rats. We hypothesize that MRI-based HDM-LD segmentations of the rat hippocampus will be at least as precise and reproducible as manual hippocampal segmentations.

MATERIALS AND METHODS

Animals

In-bred 7-week-old male nonepileptic Wistar rats from the breeding colony at the involved hospital were used. All procedures on live animals were approved by the Ethics Committees of the involved institutions.

MR Image Acquisitions

MR images were acquired on a 4.7 Tesla (T) Bruker Biospec 47/30 Avance small-animal spectrometer (Ettlingen, Germany) using a shielded-gradient set (Bruker Biospec) appropriate for rats. Radiofrequency (RF) pulse transmission and MR data acquisition were performed using a 72-mm inner-diameter birdcage coil (Bruker Biospec) optimally tuned to the ^1H frequency. T_2 -weighted axial structural images were obtained contiguously through the entire brain, using a fast spin-echo sequence (acquisition time, 298 s; repetition time, 3.1 s; echo time [TE], 67.5 ms; matrix, 256×256 ; numerical aperture, 3; field of view, $6 \text{ cm} \times 6 \text{ cm}$; voxel dimensions $0.234375 \text{ mm} \times 0.234375 \text{ mm} \times 0.5 \text{ mm}$; rapid acquisition with relaxation enhancement (rare) factor, 8). Animals were scanned under anesthesia in the prone position in a custom-built Plexiglas holder to ensure consistent positioning of the animal. Rats were anesthetized with 5% isoflurane in 1:1 air/oxygen and then maintained on 1.5–2.5% isoflurane for the remainder of the experiment. Images were collected using Paravision 3.0 (Bruker Biospec).

Postacquisition MR Image Processing

MRI acquisitions from six rats were used. One MRI data set, selected randomly, was used to construct an “atlas” image. The other five MRI data sets were used as “target” images for deformation-based hippocampal segmentation, as well as for manual hippocampal segmentation. Analyze AVW version 7.0 (Rochester, MN) was used as the software package for initial image processing. MR images were cropped and converted to an isotropic voxel dimension of 0.1171875. The intensities of the MRI dataset used for the “atlas” image were adjusted, using visual inspection, for optimal contrast of gray and white matter structures, and converted from 16-bit to 8-bit intensity ranges. The range of inclusive intensities was 3,750–16,000 for the 16-bit images, which were converted to a range of 0–255 for the 8-bit images. The intensity ranges of the additional 5 target images were then also converted from 16-bit to 8-bit images, using the same inclusive intensity ranges as the “atlas” image.

For construction of the atlas hippocampal surface image, the hippocampus was segmented, with verification in the coronal, sagittal, and horizontal planes, following the neuroanatomical boundaries of the hippocampus as described by Paxinos and Watson (20) by a single investigator. The final atlas segmentation was reviewed by a second expert segmenter for verification of the surface anatomical boundaries of the hippocampi. The segmentations were saved as binary files.

Subsequent image processing steps were performed using proprietary Linux-based software. To create the hippocampal atlas, hippocampal surface images were created by rescaling the intensity maps of the binary files, with a subsequent single iteration of a surface “smoothing” function. For deformation-based segmentations, the five “target” MR data sets underwent preprocessing in preparation for the mapping algorithm. This consisted of two steps: global landmarking and hippocampus-specific landmarking. Figure 1 shows a

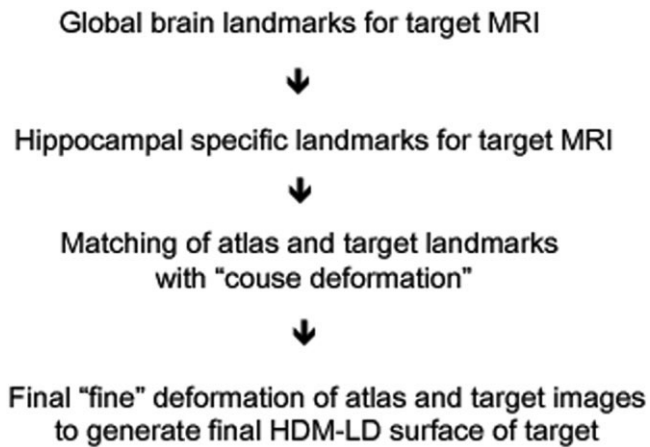


Figure 1. The figure shows a diagram of the overall steps of processing for the landmarking and deformation segmentation of the hippocampi of the target MRI studies.

diagram outlining the steps of landmarking and deformation mapping of the hippocampal surface of the target MRI.

Landmarking provided an initial condition for the intensity-matching algorithm by roughly aligning the rat and atlas scans. The first step in landmarking was identifying global landmarks which scale and align the atlas brain to the target brain, relying principally on alignment of the borders of the hemispheres, using global landmarks. The second step was individually landmarking each hippocampus. This was done by first identifying and landmarking the septal and temporal pole of each hippocampus (21), which specifies an axis for frame of reference for landmarking of each hippocampus. Then, four landmarks were identified on five cross-sections equally spaced along this axis. The landmarks were placed on the medial, lateral, superior, and inferior border of the hippocampus on each cross-section. Figure 2 shows an illustration of the 4 landmarks in one of the oblique planes. The oblique plane was generated by the algorithm after landmarking of the temporal and septal pole of the hippocampus.

Images and landmarking data were then integrated into another Linux-based software program. Within this program, the mapping algorithm used a *coarse-to-fine* procedure for generating a transformation field from an atlas reference MR to the target MR. The "coarse" aspect of the procedure relied on the landmark information provided by the expert segmenter to provide an initial low-dimensional coregistration of atlas and target images (22). The landmark information was provided in the form of the global and hippocampus-specific landmarks described in the previous section which was used to derive a coarse manifold transformation (23) from the atlas to the target images. Therefore, the initial "course" step principally consisted of aligning landmarks between the atlas and target images.

Having completed the course first step in the transformation, the volumes were roughly aligned and attention focused on the fine features of the substructures. The "fine" procedure involved the next two steps. The

second step was to solve the registration problem using a linear elastic basis formulation and the full volume data, as previously described (11,24). This was fully automatic and only driven by the volume data itself. The 3D whole brain maps corresponded to the maximizer, whose variation solution corresponded to a solution of a nonlinear partial differential equation (PDE), consisting of between 10^7 and 10^8 parameters. The third and final step of the algorithm was to solve the nonlinear PDE corresponding to the Bayesian maximizer associated with the fluid formulation at each voxel of the full volume (10,25,26).

The surfaces that were first created using the marching cubes algorithm tended to have highly nonuniform triangles. Refinement toward a more uniform surface was needed so that other computations on the surfaces could be performed, and this procedure was given by Joshi et al (27). Briefly, an elastic energy function was defined on the original surface vertices based on the distance between neighboring vertices. Minimizing this energy function would result in a surface whose vertices are more uniformly distributed across the entire surface, therefore giving the smoother appearance. Because the minimization involving spatial derivatives was performed on the local tangent planes at each vertex, the overall shape characteristic was preserved.

For the deformation-based segmentations, each target data set was completely preprocessed with landmarking twice by a single investigator, at an interval of one month, and processed using the deformation-based algorithm to generate two separate sets of deformation-based segmentations, designated as A1 and A2.

Two investigators independently performed manual segmentations of the hippocampi of the five target MR datasets. The segmentations were designated as M1 and M2.

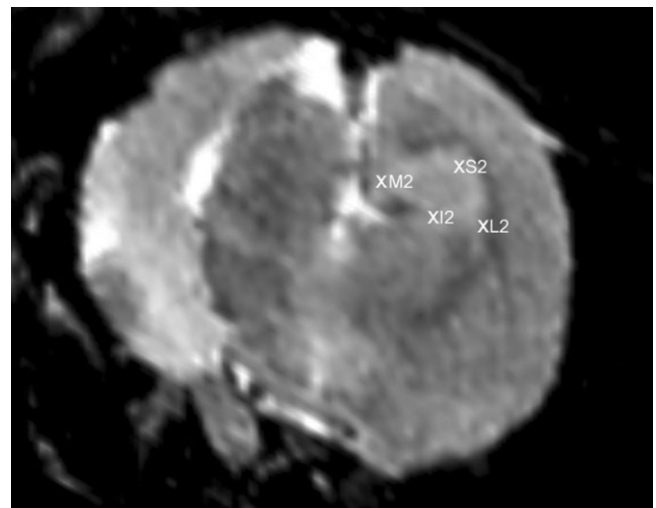


Figure 2. The figure illustrates landmarks, which are placed in an oblique MRI plane. The plane of display was generated from the algorithm after placement of the landmarks for the temporal and septal poles of the hippocampus. Landmarks are labeled M (medial), I (inferior), L (lateral), and S (superior). The number 2 designates that this is the second of five oblique landmarking planes generated by the algorithm.

Table 1
Comparison of Percentage Overlap of Voxels Between Segmentations

| Hippocampus | First Versus Second Automatic Segmentations (A1 vs. A2) | First Automatic Versus First Manual Segmentations (A1 vs. M1) |
|--------------------|---|---|
| 1R | 95.8 | 88.7 |
| 2R | 90.7 | 92.9 |
| 3R | 93.2 | 93.6 |
| 4R | 95.6 | 90.8 |
| 5R | 96.3 | 91.3 |
| 1L | 91.4 | 92.8 |
| 2L | 95.1 | 90.6 |
| 3L | 94.1 | 93.7 |
| 4L | 94.9 | 91.2 |
| 5L | 96.6 | 91.4 |
| Right hippocampi | | |
| Mean | 94.3 | 91.4 |
| Standard deviation | 2.5 | 1.3 |
| Left hippocampi | | |
| Mean | 94.4 | 91.9 |
| Standard deviation | 1.0 | 1.4 |

Comparisons between two segmentations were made by computing the percentage of overlap of voxels, as in previous studies (15). One segmentation was designated the reference (R) and the other the study (S) segmentation that we compared against the reference. The percentage of overlap was computed as the number of overlapping segmented voxels between the two segmentations divided by the total number of segmented voxels in the study, that is, $(R \text{ intersect } S)/S \times 100$. We used the manual segmentations of one investigator (Y.R.L.) as the reference segmentations, and the first

series of deformation segmentations (A1) as the comparison segmentations.

RESULTS

Table 1 shows comparisons of three segmentations: two automatic segmentations (automatic segmentation 1 [A1] and automatic segmentation 2 [A2]) and one manual segmentation (manual segmentation 1 [M1]). The mean percentage overlap for the hippocampi between A1 and A2 for the right hippocampi was 94.4 (SD 1.0) and for the left hippocampi was 94.3 (SD 2.5), while the mean percentage overlap between A1 and M1 for the right hippocampi was 91.4 (SD 1.3) and for the left hippocampi was 91.9 (SD 1.4).

Table 2 shows volume measurements based on the four segmentations. Mean values for absolute percentage differences for comparisons of all the segmentations were the following: A1 versus A2, 3.2 (SD 1.0); M1 versus M2, 6.82 (SD 5.22); A1 versus M1, 13.0 (SD 1.8).

Figure 3 shows coronal sections of a randomly selected rat MRI (MRI 2) taken at approximately 1-mm intervals. Figure 3A–E progresses from a rostral to caudal direction, with the white shading representing the manual segmentation, and the line representing the automated segmentation. The major differences in the segmentation are represented in Figure 3C, which represents the region where the axis of the hippocampus changes in direction. Figure 3F–J is a replication of the MRI sections shown in Figure 3A–E, without superimposed automated segmentations.

Figures 4–6 show illustrations of the HDM-LD surface images of hippocampi from a single rat MRI. Figure 4 shows a 3D representation of the surface of the hippocampi (Fig. 4D), with associated 2D MR images in the

Table 2
Volume Measurements and Between-Method Hippocampal Volume Differences

| Hippocampus | Automatic Segmentation | | | Manual Segmentation | | | Percentage Difference Between Methods (A1 vs. M1) |
|--------------------|------------------------------|------------------------------|--------------------------------|------------------------------|------------------------------|--------------------------------|---|
| | A1 Volume (mm ³) | A2 Volume (mm ³) | Absolute Percentage Difference | M1 Volume (mm ³) | M2 Volume (mm ³) | Absolute Percentage Difference | |
| 1 R | 34.46 | 31.53 | 8.5 | 37.25 | 37.78 | 1.4 | 8.1 |
| 2R | 30.62 | 31.84 | 3.4 | 35.84 | 38.73 | 8.1 | 14.6 |
| 3R | 35.15 | 34.76 | 1.1 | 40.64 | 34.24 | 15.7 | 13.5 |
| 4R | 31.90 | 31.46 | 1.4 | 36.83 | 36.32 | 1.4 | 13.4 |
| 5R | 30.22 | 29.18 | 3.4 | 34.30 | 32.91 | 4.0 | 11.9 |
| 1L | 31.35 | 30.26 | 3.5 | 37.15 | 35.71 | 1.5 | 15.6 |
| 2L | 32.8 | 32.16 | 2.0 | 36.43 | 40.22 | 10.4 | 10 |
| 3L | 33.19 | 34.11 | 2.7 | 38.90 | 33.66 | 13.5 | 14.9 |
| 4L | 31.71 | 31.01 | 2.2 | 36.19 | 35.04 | 3.2 | 12.4 |
| 5L | 29.95 | 28.74 | 4.0 | 35.28 | 32.12 | 9.0 | 15.1 |
| Right hippocampi | | | | | | | |
| Mean | 32.47 | 31.76 | 3.6 | 36.97 | 36.00 | 6.1 | 12.3 |
| Standard deviation | 2.23 | 2.29 | 1.3 | 2.70 | 2.54 | 6.2 | 1.1 |
| Left hippocampi | | | | | | | |
| Mean | 31.80 | 31.26 | 2.88 | 36.79 | 35.35 | 7.51 | 13.6 |
| Standard deviation | 1.45 | 2.25 | 0.93 | 1.54 | 3.52 | 4.3 | 2.4 |
| Overall | | | | | | | |
| Mean | 32.14 | 31.50 | 3.2 | 36.88 | 35.67 | 6.82 | 13.0 |
| Standard deviation | 1.64 | 2.02 | 1.0 | 1.91 | 2.66 | 5.22 | 1.81 |

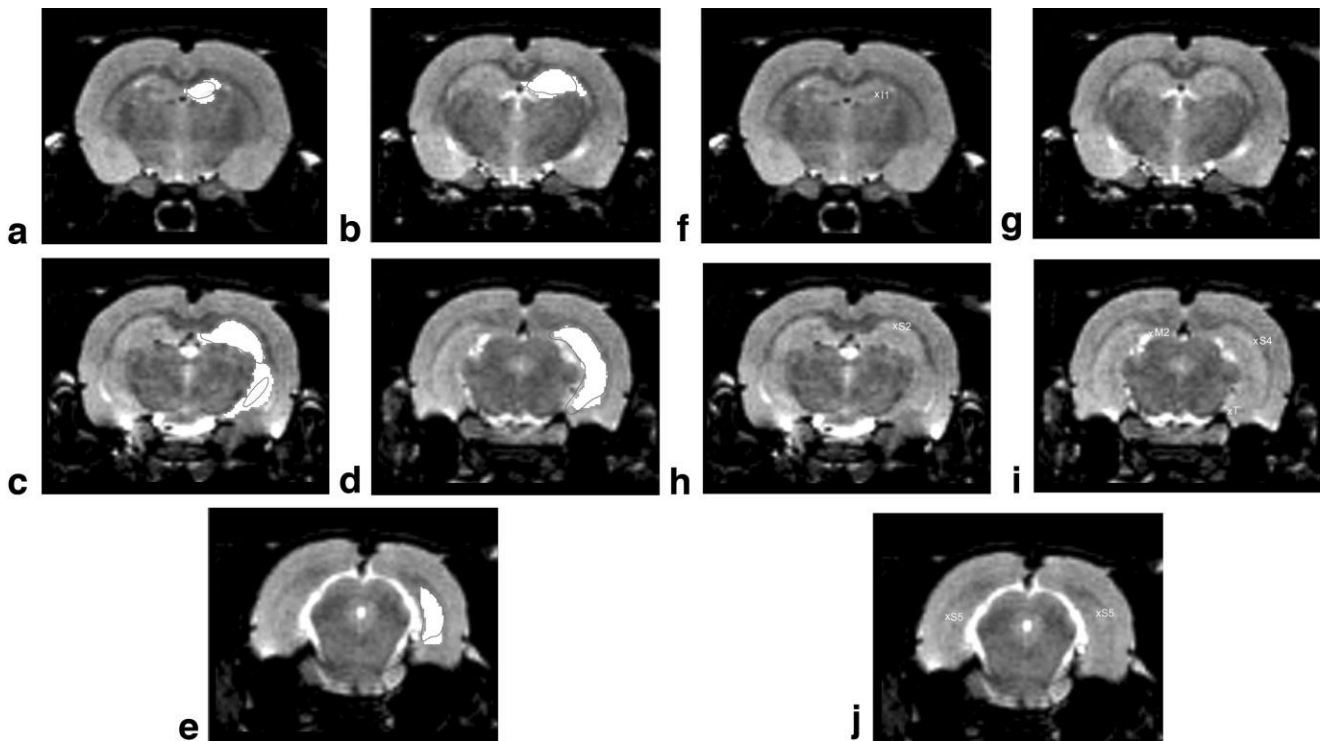


Figure 3. Coronal sections of a randomly selected rat T_2 -weighted image (MRI 2) taken at approximately 1-mm intervals. **a–e:** The surface outline in each section represents the deformation segmentation, while the white shaded area represents the manual segmentation. The MRI Figure 3A shows the anterior region of the dorsal pole of the hippocampus, with subsequent images A–E moving to posterior segments of the hippocampus. The MR images A–F are reproduced as images **f–j**, without superimposed segmentations to allow for better visual inspection of the MRI itself. Images F–J also show landmarks used for the deformation segmentations. Not all landmarks are visible because the deformation algorithm specifies oblique planes for landmarking, as shown in Figure 2. Regions of overlap of segmentations, as shown in A–E, are relatively consistent, with the exception of 3C, which shows greater mismatch of the deformation and manual segmentations. In this region of the hippocampus, the long axis of the hippocampus rotates to run relatively parallel to the coronal plane, and the borders of the hippocampus are less-defined on the MR images, making precise definition of the hippocampal boundary more difficult.

coronal (Fig. 4A), horizontal (Fig. 4B), and sagittal (Fig. 4C) planes. In Figure 4D, the hippocampi are viewed from a rostral perspective. The red marker is placed on the septal pole of the right hippocampus.

Figure 5 shows a 3D view of the hippocampi from a caudal perspective, viewing the surface from the opposite direction as presented in Figure 4.

Figure 6 shows a 3D view of the hippocampi, with the surfaces rotated to show the lateral surface of the left hippocampus. This view serves to show the “C” shape of the left hippocampus.

DISCUSSION

Past techniques used to quantitate the volume and shape of the hippocampus from MR images of rats have focused on defining structures in a single 2D plane for volumetric measurements (4,7). Using HDM-LD with general pattern matching, anatomic structures can be segmented using global shape models. By representing the typical structures by means of the construction of templates, and their variability by the definition of transformations applied to the templates, MR images of the hippocampus may be semiautomatically segmented (28). HDM-LD offers advantages over 2D plane reconstructions by providing 3D representations of the in-

cluded segmented structure, and allowing mathematical comparisons of surface structure between different images (29).

There has been extensive validation of MRI-based HDM-LD techniques in human subjects (14–16). However, HDM-LD techniques have not previously been applied in the rat brain. The relatively smaller size of the rat brain, and resultant limitations in image resolution of rat brain MRI studies are issues in applying MRI-based HDM-LD. However, with improvements in MRI rat brain imaging, and our current protocol of acquiring high-resolution volumetric images on a 4.7T animal MRI scanner, application of HDM-LD in the rat has become a practical proposition.

The rat hippocampus is a good target for HDM-LD, as it is relatively well demarcated on our MRI acquisitions, and is one of the relatively larger structures in the rat brain. The 3D surface anatomy, however, is relatively complex, with the long axis of the structure turning at an approximately 90 degree angle between the septal and temporal poles of the hippocampus, and therefore running in relatively perpendicular planes at either end of the structure, which is best illustrated in Figure 6. The hippocampus extends from the basal forebrain, over the diencephalon, and caudoventrally into the temporal lobe. The septal pole is located dorsally and

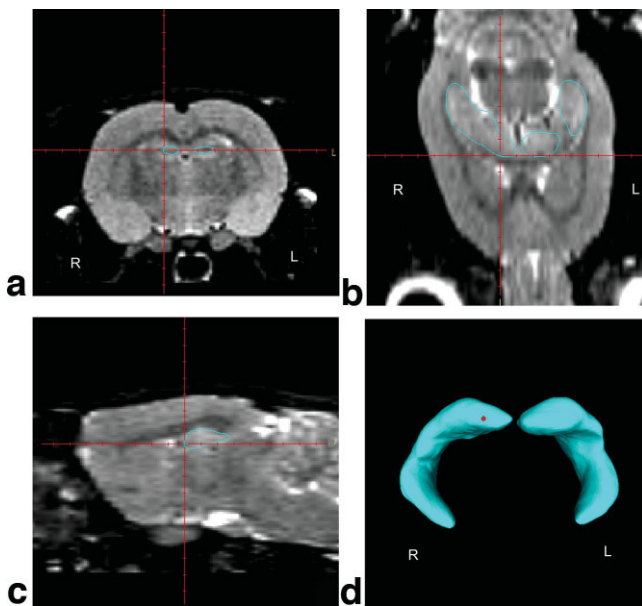


Figure 4. a–d: A three-dimensional representation of the surface of the hippocampi (D), with associated two-dimensional MR images in the coronal (A), horizontal (B), and sagittal (C) planes. A marker is placed over the rostral aspect of the septal pole of the right hippocampus, which corresponds to the intersection of the crosshairs on two-dimensional images. Hippocampal surface outlines are presented on A–C. In D, the hippocampi are viewed from a rostral position, with the temporal pole projecting to the lower part of the image.

rostrally, while the temporal pole is located caudally and ventrally (21). There remain differences in terminology for rat hippocampal structures, while the septal pole is also referred to as the dorsal pole, and the temporal pole is also referred to as the ventral pole (30). The long axis of the hippocampal formation is referred to as the septotemporal axis.

In this study, we show that the results of HDM-LD segmentations and manual segmentations of the rat hippocampus showed good correlations with percentage overlap of structures. The average overlap of the two separate automatic segmentations (A1 and A2) as well as the automatic (A1) and manual (M1) segmentations (Table 1) was better than 90% average overlap for both

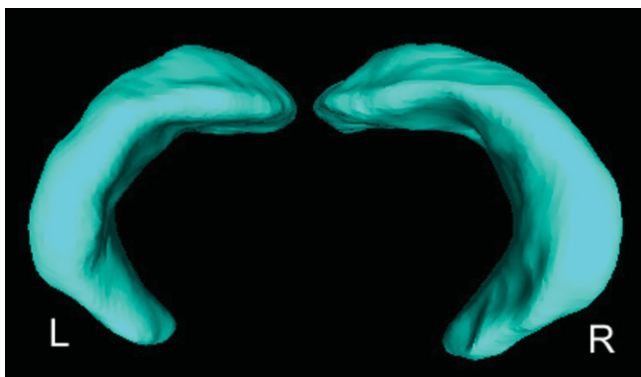


Figure 5. The figure shows a three-dimensional view of the hippocampi from a caudal view point.

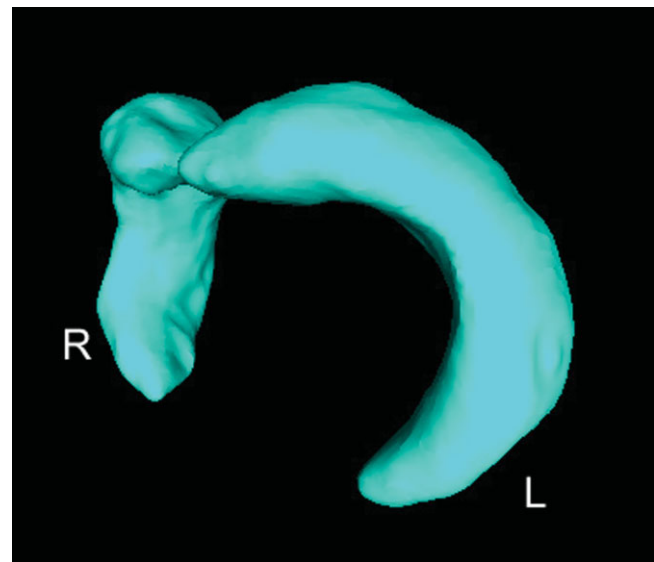


Figure 6. The figure shows a three-dimensional view of the hippocampi, with both hippocampi slightly rotated to the right, with the left hippocampus in the foreground. This view shows the lateral surface of the left hippocampus, and illustrates the “C” shaped structure of the hippocampus.

right and left hippocampi. This helps to verify that the segmentations occupy the same 3D space. Overlap results between segmentations are comparable to those from HDM-LD studies performed in human subjects (15). Volume comparisons (Table 2) show slightly lower average absolute percentage volume differences between the deformation segmentations compared to the manual segmentations. This finding would suggest that the reproducibility of volume measurements using HDM-LD is comparable, if not slightly better, than repeated manual segmentation measurements. However, there are relatively larger volume differences in direct comparison of the deformation and manual segmentation (A1 versus M1), with the manual segmentations showing a consistently larger volume. Figure 1 shows a comparison of the deformation and manual segmentation. Although overlap of the segmentation is good (as indicated in the data of Table 1), there are regions at the margins of the hippocampal borders where there are greater discrepancies in the two measurements. On the MR images, the hippocampal borders as the hippocampus extends ventrocaudally into the temporal lobe (as in Fig. 3C) were often the most difficult to define due to lack of clearly defined boundaries with surrounding structures. As in past validation studies with HDM-LD (15), there is difficulty in defining hippocampal borders, with either the deformation or manual segmentation technique, where hippocampal boundaries are most poorly defined on the MRI images. In general, our results are most consistent with good overlap between the segmentations, showing that both sets of segmentations cover similar regions, but with the manual segmentations being slightly larger, likely related to slightly greater volume inclusion of the manual segmentations at the margins of the segmentations.

The relative size of the rat hippocampus also likely plays a role in our validation results. Past studies have

shown greater percentage error when segmentations involve smaller volumes (31). In a study of progressive multiple sclerosis MR lesions, Goodkin et al found a coefficient of variation for three successive lesion measurements inversely related to the lesion area, ranging from 22.6% for lesion less than 0.67 cm² to 12.1% for larger lesions (31). Previous authors have used logarithmic comparisons to account for percentage volume differences in structures that are of significantly different size (32).

Whereas the hippocampus is grossly relatively well-defined on MR images, enabling a surface reconstruction using HDM-LD, different regions of the hippocampus along the septotemporal axis are composed of distinctly different subfields (21). For example, near the septal pole, only the dentate gyrus and the CA1-3 subdivisions of the hippocampus are present. Moving from the septal pole approximately 15% of the way back toward the temporal pole, the subiculum appears. Therefore, different subregions of the hippocampus are represented uniquely along segments of the hippocampal surface. Investigators have established multimodal, multidimensional animal brain atlases to study these complex relationships (33). By creating mathematically defined, high resolution surfaces, HDM-LD segmentations will also offer possible avenues for studying relationships of surface anatomical changes correlating to hippocampal subfields. Changes in hippocampal surfaces can be compared between groups, or longitudinally over time within subjects or groups of subjects.

We selected acquisition parameters for the rat MRI studies, including the TE = 67.5 ms, which would maximize contrast within the image, with a minimal acquisition period. Whereas past HDM-LD segmentation protocols have used T1-weighted images (14,15), any image sequence that produces high-resolution volumetric images and provides good contrast of structures will theoretically work for HDM-LD segmentation. The current study shows that images with relative T2 weighting can also yield good HDM-LD segmentations.

Based on the methods of previous validation studies (15,16), and the difficulties in accurate manual hippocampal segmentation of high-resolution, interpolated datasets (which typically take 2–3 h per hippocampus in our experience), we chose to limit the number of MRI datasets for our analysis. There is some ambiguity in defining borders of neuroanatomical structures on MRI (i.e., as discussed above where the hippocampus extends ventrocaudally into the temporal lobe). Therefore, interpretation of the definitive accuracy of MRI-based segmentations is difficult. Because of these factors, we chose our current methods of segmentation overlap and comparison of segmentation methods.

In conclusion, the study validates the accuracy and reproducibility of HDM-LD segmentations of the hippocampus, showing that overlap and absolute percentage volume differences between the automated HDM-LD segmentations and high-resolution manual segmentations are comparable. HDM-LD will be a useful tool for investigating in vivo hippocampal structural changes in rat models of human disease.

ACKNOWLEDGEMENTS

Funding for this project was provided in part by the Victorian Government Transport Accident Commission (TAC) in the form of a Victorian Neurotrauma Initiative grant.

REFERENCES

- Hogan RE, Wang L, Bertrand ME, et al. MRI-based high-dimensional hippocampal mapping in mesial temporal lobe epilepsy. *Brain* 2004;127:1731–1740.
- Wang L, Joshi SC, Miller MI, Csernansky JG. Statistical analysis of hippocampal asymmetry in schizophrenia. *Neuroimage* 2001;14:531–545.
- Posener JA, Wang L, Price JL, et al. High-dimensional mapping of the hippocampus in depression. *Am J Psychiatry* 2003;160:83–89.
- Grohn O, Pitkanen A. Magnetic resonance imaging in animal models of epilepsy-noninvasive detection of structural alterations. *Epilepsia* 2007;48(Suppl 4):3–10.
- Jones NC, Salzberg MR, Kumar G, Couper A, Morris MJ, O'Brien TJ. Elevated anxiety and depressive-like behavior in a rat model of genetic generalized epilepsy suggesting common causation. *Exp Neurol* 2008;209:254–260.
- Watson C, Jack CR Jr, Cendes F. Volumetric magnetic resonance imaging. Clinical applications and contributions to the understanding of temporal lobe epilepsy. *Arch Neurol* 1997;54:1521–1531.
- Jupp B, Williams JP, Tesiram YA, Vosmansky M, O'Brien TJ. Hippocampal T signal change during amygdala kindling epileptogenesis. *Epilepsia* 2006;47:41–46.
- Cendes F, Leproux F, Melanson D, et al. MRI of amygdala and hippocampus in temporal lobe epilepsy. *J Comput Assist Tomogr* 1993;17:206–210.
- Grenander U. Elements of pattern theory. London: Johns Hopkins University Press; 1996. 210 p.
- Christensen GE, Rabbitt RD, Miller MI. A deformable neuroanatomy textbook based on viscous fluid mechanics. In: Prince J, editor. In: Proceedings of the 27th Annual Conference on Information Sciences and Systems. Baltimore: The Johns Hopkins University; 1993. p 211–216.
- Miller MI, Christensen GE, Amit Y, Grenander U. Mathematical textbook for deformable neuroanatomies. *Proc Natl Acad Sci U S A* 1993;90:11944–11948.
- Miller MI, Grenander U. Computational anatomy: an emerging discipline. *Q Appl Math* 1998;5:617–694.
- Gardner R, Hogan RE. Three-dimensional deformation-based hippocampal surface anatomy, projected on MRI images. *Clin Anat* 2005;18:481–487.
- Haller JW, Christensen GE, Joshi SC, et al. Hippocampal MR imaging morphometry by means of general pattern matching. *Radiology* 1996;199:787–791.
- Hogan RE, Mark KE, Wang L, Joshi S, Miller MI, Bucholz RD. Mesial temporal sclerosis and temporal lobe epilepsy: MR imaging deformation-based segmentation of the hippocampus in five patients. *Radiology* 2000;216:291–297.
- Haller JW, Banerjee A, Christensen GE, et al. Three-dimensional hippocampal MR morphometry with high-dimensional transformation of a neuroanatomic atlas. *Radiology* 1997;202:504–510.
- Csernansky JG, Joshi S, Wang L, et al. Hippocampal morphometry in schizophrenia by high dimensional brain mapping. *Proc Natl Acad Sci U S A* 1998;95:11406–11411.
- Wang L, Swank JS, Glick IE, et al. Changes in hippocampal volume and shape across time distinguish dementia of the Alzheimer type from healthy aging. *Neuroimage* 2003;20:667–682.
- Hogan RE, Carne RP, Kilpatrick CJ, et al. Hippocampal deformation mapping in MRI-negative PET-positive temporal lobe epilepsy. *J Neurol Neurosurg Psychiatry* 2008;79:636–640.
- Paxinos G, Watson C. The rat brain in stereotaxic coordinates. 4th edition. San Diego, CA: Academic Press; 1998. 162 p.
- Witter MP, Amaral DG. Hippocampal formation. In: Paxinos G, editor. The rat nervous system. 3rd edition. Boston: Elsevier Academic Press; 2004. p 635–704.
- Joshi S. Large deformation diffeomorphisms and gaussian random fields for statistical characterization of brain submanifolds [dissertation]. Washington University, Saint Louis; 1997.

23. Joshi SC, Miller MI, Christensen GE, Banerjee A, Coogan TA, Grenander U. Hierarchical brain mapping via a generalized Dirichlet solution for mapping brain manifolds. *Proc SPIE Inter Symp Opt Sci Eng Instrum* 1995;2573:278–289.
24. Christensen GE, Rabbitt RD, Miller MI. (3D) Brain mapping using a deformable neuroanatomy. *Phys Med Biol* 1994;39:609–618.
25. Christensen GE, Rabbitt RD, Miller MI, Joshi SC, Grenander U, Coogan TA. Topological properties of smooth anatomic maps. *Information processing in medical imaging*. Netherlands: IPMI; 1995. p 101–112.
26. Christensen GE, Joshi SC, Miller MI. Volumetric transformation of brain anatomy. *IEEE Trans Med Imaging* 1997;16:864–877.
27. Joshi S, Miller MI, Grenander U. On the geometry and shape of brain sub-manifolds. *Int J Pattern Recognit Artif Intell* 1997;11:1317–1343.
28. Hogan RE, Bucholz RD, Joshi S. Hippocampal deformation-based shape analysis in epilepsy and unilateral mesial temporal sclerosis. *Epilepsia* 2003;44:800–806.
29. Hogan RE, Wang L, Bertrand ME, et al. Predictive value of hippocampal MR imaging-based high-dimensional mapping in mesial temporal epilepsy: preliminary findings. *AJNR Am J Neuroradiol* 2006;27:2149–2154.
30. Sasaki M, Tohyama K, Matsunaga S, et al. MRI identification of dorsal hippocampus homologue in human brain. *Neuroreport* 2004;15:2173–2176.
31. Goodkin DE, Ross JS, Medendorp SV, Konecni J, Rudick RA. Magnetic resonance imaging lesion enlargement in multiple sclerosis. Disease-related activity, chance occurrence, or measurement artifact? *Arch Neurol* 1992;49:261–263.
32. Bartzokis G, Altshuler LL, Greider T, Curran J, Keen B, Dixon WJ. Reliability of medial temporal lobe volume measurements using reformatted 3D images. *Psychiatry Res* 1998;82:11–24.
33. MacKenzie-Graham AJ, Lee EF, Dinov ID, Yuan H, Jacobs RE, Toga AW. Multimodal, multidimensional models of mouse brain. *Epilepsia* 2007;48(Suppl 4):75–81.